Molecular Human Reproduction, pp. 1–10, 2017
doi:10.1093/molehr/gax062

molecular human reproduction

ORIGINAL ARTICLE

Semi-automatized segmentation method using image-based flow cytometry to study sperm physiology: the case of capacitation-induced tyrosine phosphorylation

Arturo Matamoros-Volante[1], Ayelen Moreno-Irusta[2,3], Paulina Torres-Rodriguez[1], Laura Giojalas[2,3], María G. Gervasi[4], Pablo E. Visconti[4], and Claudia L. Treviño[1,*]

[1]Departamento de Genética del Desarrollo y Fisiología Molecular, Instituto de Biotecnología, Universidad Nacional Autónoma de México, Cuernavaca, Morelos 62250, Mexico [2]Universidad Nacional de Córdoba (UNC), Facultad de Ciencias Exactas, Físicas y Naturales, Centro de Biología Celular y Molecular, Córdoba, Argentina [3]Consejo de Investigaciones Científicas y Técnicas (CONICET), Instituto de Investigaciones Biológicas y Tecnológicas, Córdoba, Argentina [4]Department of Veterinary and Animal Sciences, University of Massachusetts, Amherst, MA, USA

*Correspondence address. Departamento de Genética del Desarrollo y Fisiología Molecular, Instituto de Biotecnología, Universidad Nacional Autónoma de México, Cuernavaca, Morelos 62250, Mexico. Email: ctrevino@ibt.unam.mx

Submitted on October 20, 2017; resubmitted on November 6, 2017; editorial decision on November 17, 2017; accepted on November 21, 2017

STUDY QUESTION: Is image-based flow cytometry a useful tool to study intracellular events in human sperm such as protein tyrosine phosphorylation or signaling processes?

SUMMARY ANSWER: Image-based flow cytometry is a powerful tool to study intracellular events in a relevant number of sperm cells, which enables a robust statistical analysis providing spatial resolution in terms of the specific subcellular localization of the labeling.

WHAT IS KNOWN ALREADY: Sperm capacitation is required for fertilization. During this process, spermatozoa undergo numerous physiological changes, via activation of different signaling pathways, which are not completely understood. Classical approaches for studying sperm physiology include conventional microscopy, flow cytometry and Western blotting. These techniques present disadvantages for obtaining detailed subcellular information of signaling pathways in a relevant number of cells. This work describes a new semi-automatized analysis using image-based flow cytometry which enables the study, at the subcellular and population levels, of different sperm parameters associated with signaling. The increase in protein tyrosine phosphorylation during capacitation is presented as an example.

STUDY DESIGN SIZE, DURATION: Sperm cells were isolated from seminal plasma by the swim-up technique. We evaluated the intensity and distribution of protein tyrosine phosphorylation in sperm incubated in non-capacitation and capacitation-supporting media for 1 and 18 h under different experimental conditions. We used an antibody against FER kinase and pharmacological inhibitors in an attempt to identify the kinases involved in protein tyrosine phosphorylation during human sperm capacitation.

PARTICIPANTS/MATERIALS, SETTING, METHODS: Semen samples from normospermic donors were obtained by masturbation after 2–3 days of sexual abstinence. We used the innovative technique image-based flow cytometry and image analysis tools to segment individual images of spermatozoa. We evaluated and quantified the regions of sperm where protein tyrosine phosphorylation takes place at the subcellular level in a large number of cells. We also used immunocytochemistry and Western blot analysis. Independent experiments were performed with semen samples from seven different donors.

MAIN RESULTS AND THE ROLE OF CHANCE: Using image analysis tools, we developed a completely novel semi-automatic strategy useful for segmenting thousands of individual cell images obtained using image-based flow cytometry. Contrary to immunofluorescence which relies on the analysis of a limited sperm population and also on the observer, image-based flow cytometry allows for unbiased quantification and simultaneous localization of post-translational changes in an extended sperm population. Interestingly, important data can be

independently analyzed by looking to the frame of interest. As an example, we evaluated the capacitation-associated increase in tyrosine phosphorylation in sperm incubated in non-capacitation and capacitation-supporting media for 1 and 18 h. As previously reported, protein tyrosine phosphorylation increases in a time-depending manner, but our method revealed that this increase occurs differentially among distinct sperm segments. FER kinase is reported to be the enzyme responsible for the increase in protein tyrosine phosphorylation in mouse sperm. Our Western blot analysis revealed for the first time the presence of this enzyme in human sperm. Using our segmentation strategy, we aimed to quantify the effect of pharmacological inhibition of FER kinase and found a marked reduction of protein tyrosine phosphorylation only in the flagellum, which corresponded to the physical localization of FER in human sperm. Our method provides an alternative strategy to study signaling markers associated with capacitation, such as protein tyrosine phosphorylation, in a fast and quantitative manner.

LARGE SCALE DATA: None.

LIMITATIONS REASONS FOR CAUTION: This is an *in vitro* study performed under controlled conditions. Chemical inhibitors are not completely specific for the intended target; the possibility of side effects cannot be discarded.

WIDER IMPLICATIONS OF THE FINDINGS: Our results demonstrate that the use of image-based flow cytometry is a very powerful tool to study sperm physiology. A large number of cells can be easily analyzed and information at the subcellular level can be obtained. As the segmentation process works with bright-field images, it can be extended to study expression of other proteins of interest using different antibodies or it can be used in living sperm to study intracellular parameters that can be followed using fluorescent dyes sensitive to the parameter of interest (e.g. pH, Ca^{2+}). Therefore, this a versatile method that can be exploited to study several aspects of sperm physiology.

STUDY FUNDING AND COMPETING INTEREST(S): This work was supported DGAPA (IN203116 to C. Treviño), Fronteras-CONACyT No. 71 and Eunice Kennedy Shriver National Institute of Child Health and Human Development NIH (RO1 HD38082) to P.E. Visconti and by a Lalor Foundation fellowship to M.G. Gervasi. A. Matamoros is a student of the Maestría en Ciencias Bioquímicas-UNAM program supported by CONACyT (416400) and DGAPA-UNAM. A. Moreno obtained a scholarship from Red MacroUniversidades and L. Giojalas obtained a schloarhip from CONICET and Universidad Nacional de Cordoba. The authors declare there are not conflicts of interest.

Key words: image-based flow cytometry / sperm image segmentation / sperm capacitation / protein tyrosine phosphorylation / FER kinase / PYK2

Introduction

After ejaculation in the female tract and in order to acquire fertilizing ability, sperm must undergo a maturation process known as capacitation (Austin, 1951; Chang, 1951). Nevertheless, the signaling pathways responsible to produce capacitation in human spermatozoa are not completely understood. The fact that sperm cells exhibit a high degree of variability and that each ejaculate contains a very large number of cells, complicates their study. To build a signaling network, a reliable and quantitative method to study signaling pathways is necessary. In the present work, we implemented a segmentation process based on image-based flow cytometry data to provide a new semi-automatized analysis to quantify sperm physiological parameters and localize post-translational changes in mammalian sperm in general. This methodology can be used to determine and quantify many intracellular parameters as fluorescent detectors present in the image-based flow cytometer (up to 9 in AMNIS ImageStream Mark II) in thousands of individual spermatozoa. For example, Western Blot has been the preferred technique to investigate capacitation-associated tyrosine phosphorylation (pY), but it provides only the average information of a cell population. Immunocytochemistry has also been applied to determine the sites of signaling processes at the subcellular level, but only a small number of cells can be captured and analyzed manually, which is time-consuming and the quantification of the signal could be biased by the investigator.

The increase in pY represents one of the most important process during capacitation and has been considered as a capacitation marker. While traveling through the female reproductive tract, sperm undergo a rapid increase in $[Ca^{2+}]_i$ and HCO_3^-, which stimulates a signaling cascade that includes an increase in protein kinase A (PKA) activity with a consequent serine/threonine protein phosphorylation (pS/T) (Visconti *et al.*, 2011) and pY by a mechanism not yet clearly defined. Although several approaches have been used to identify these proteins, the particular set of kinases involved in this process is far from clear. Recently, a genetic and pharmacological study by our group (Alvau *et al.*, 2016) demonstrated that FERT kinase plays a major role during mouse sperm pY, although several other candidates have been previously proposed. Since it is not possible to extrapolate findings among species and genetic studies cannot be performed in sperm cells, biochemical and pharmacological approaches are the best tools to dissect the signaling cascades responsible for pY in these cells. Image-based flow cytometry is a novel and powerful technique that provides subcellular information of the cell parameters (i.e. quantification of fluorescence intensity) allowing the analysis of a large number of cells. This technique has been applied to non-human sperm scarcely (Kennedy *et al.*, 2014; Santiani *et al.*, 2016).

We used this technique in an attempt to identify some of the kinase (s) involved in the process of pY, by means of inhibitors, confirming that PYK2 (Battistone *et al.*, 2014) and FERT kinases, but not FAK, participate in the pY cascade during human sperm capacitation, in contrast to what was reported in mouse sperm where FER, but not PYK2, was involved. We also provide the first evidence of expression and subcellular localization of FER in human spermatozoa, which contributes with additional information for building complete signaling network associated to capacitation. The method developed in this work represents the first attempt to use and unbiased methodological approach to investigate localization of a signal transduction marker in sperm.

Materials and Methods

Materials

Chemicals were purchased from various sources: Potassium dihydrogen phosphate (KH_2PO_4) and anhydrous glucose were obtained from J.T. Baker (USA). Bovine serum albumin (BSA) was purchased from US Biological (USA). Paraformaldehyde form Ted Pella, Inc. (USA). PF573228 and were obtained from Selleck Biochem (USA). All other chemicals were purchased from Sigma-Aldrich (USA). Mouse monoclonal anti-FER (cat #4268) was purchased from Cell Signaling Technology (USA). Mouse monoclonal anti-phosphotyrosine (anti-PY) antibody (clone 4G10, cat #05–321) was obtained from EMD Millipore (Germany). Alexa Fluor 488-conjugated anti-mouse secondary antibody was purchased from Invitrogen (Thermo Fisher Scientific, USA), and peroxidase/conjugated anti-mouse IgG was obtained from Jackson Immuno Research (USA).

Culture media

The non-capacitating (NC) media used in this study was the modified BWW which contained (in mM): NaCl 120, KCl 4.8, $CaCl_2$ 0.22, $MgSO_4$ 1.16, KH_2PO_4 1.16, glucose 5, Na-pyruvate 0.2, Na-lactate 11.7, Hepes 45 and gentamicin 8% (*w*/*v*). For capacitating conditions, the media was supplemented with (in mM): $NaHCO_3$ 25, $CaCl_2$ 1.68 and BSA 3% (*w*/*v*), and osmolarity was adjusted reducing NaCl concentration to 88 mM. All media were adjusted to pH 7.4 and the osmolarity was maintained at around 290 mOs kg^{-1}.

Sperm samples preparation

Protocols for human sperm were approved by the Bioethics Committee of the Instituto de Biotecnología (UNAM, Mexico). Informed consent forms were signed by all donors. Sperm samples were collected by masturbation after 2 days of sexual abstinence. Only those samples exhibiting normal seminal parameters according to the WHO (2010) criteria were included in the study. Semen samples were liquefied at 37°C under an atmosphere of 5% CO_2 in air for 30 min. Spermatozoa were separated from the seminal plasma by swim up (Mata-Martínez *et al.*, 2013). Briefly, each semen sample was aliquoted in several swim-up tubes. For each tube, 500 µl of the semen sample were placed in a glass test tube and then 1 ml of BWW was gently placed on top, incubating for 1 h at 37°C under an atmosphere of 5% CO_2 in air. At the end of the incubation, 700 µl of the sperm suspension were collected from the upper part of the tube, making a pool with the volume collected from each swim-up tube. Sperm concentration was determined using a Makler Counting Chamber (Sefi Medical Instruments, Israel), adjusting the sperm concentration in BWW medium. Sperm samples were incubated at 37°C under an atmosphere of 5% CO_2 in air to promote capacitation for 17 additional hours, while non-capacitated sperm samples were incubated them in BWW medium without BSA and bicarbonate. Incubation was done in the absence or presence of kinase inhibitors: PF573228 (FAK inhibitor, 10 µM in DMSO) and PF431396 (PYK2 and FAK inhibitor, 10 µM in DMSO). Sperm viability after 18 h of capacitation was explored using both motility and staining with propidum iodide prior to fixation. Both methods revealed that sperm viability was 87% after 18 h of capacitation (data not shown).

Measurement of protein tyrosine phosphorylation (pY) using imaged-based flow cytometry

After swim up, the cells were incubated for 1 h (either in capacitating or NC conditions) and for 18 h under capacitating conditions. Then, the samples were centrifuged at 200 *g* for 3 min and the pellet resuspended in 1 mL of PBS, adjusting the cell concentration to 10×10^6 cells/ml. Spermatozoa were fixed with 2% (*v*/*v*) paraformaldehyde in PBS for 20 min at room temperature, washed, and then treated with 0.05% Triton X-100 in PBS for 15 min. Samples were then centrifuged at 4000 *g* in PBS for 5 min. The sperm pellet was resuspended in 1 ml of blocking solution (3% (*w*/*v*) BSA in PBS) for 2 h at room temperature. The incubation with the first antibody (anti-phophotyrosine monoclonal antibody; 1:500 dilution) was performed in 0.05% (*v*/*v*) Tween 20 in PBS (PBS-T) (supplemented with 3% (*w*/*v*) BSA) at 4°C overnight. The sample was then centrifuged at 4000 *g* in PBS for 5 min, and then incubated with Alexa-488 conjugated anti-mouse IgG antibody (1:500) diluted in PBS-T (supplemented with 3% (w/v) BSA) in the dark for 1 h at room temperature, before performing the final wash with PBS. The control samples were processed as described above, but without either the primary or secondary antibody, or both. Cell concentration was adjusted to $2–5 \times 10^6$ cells/ml in a final volume of 50 µl in PBS. pY labeling was detected using an Imaging flow cytometer ImageStream Mark II (Amnis, Seattle, WA) using ×60 magnification. For excitation light, we used 488 nm solid state laser set of variable intensity (20–50 mW) that was adjusted for each experiment to reduce autofluorescence of unstained cells. Bright-field images were collected in channel 1. The signal of Alexa 488 secondary antibody was collected in channel 2 (480–560 nm). During acquisition, area and aspect ratio thresholds (≥50–≤200 μm^2 and ≤0.3, respectively) were set to acquire events compatible with sperm morphology. Additionally, a focus threshold (Gradient RMS for channel 1 ≥ 60) was held to record focused cells only. Considering these parameters, the acquisition rate was of ~1000 to 2000 cells per minute. At least 10 000 cells were recorded for each condition.

Segmentation of sperm images

First, we developed masks to cover specific regions of human sperm. The cell images were acquired using the image-flow cytometer and analyzed with the software IDEAS. This software defines a mask as the pixels of interest to be analyzed. Using this tool, we developed complementary new masks combining existing functions in IDEAS software. These masks allowed us to separately analyze specific regions in human sperm images (head, midpiece and principal piece). The steps to create these masks are detailed below.

(1) Entire cell mask. This permits the measurement of the pixels of the entire cell. We applied the morphology function to detect the pixels that contain the image in the bright-field channel and performed a subsequent erosion of one pixel (Fig. 1A, i).
(2) Head mask. This was created using the adaptive erode function with a coefficient of 52 which is helpful to identify circular regions in an image (Fig. 1A, ii). The resulting mask was dilated by two pixels to ensure the inclusion of all the pixels that correspond to the sperm head (Fig. 1A, iii).
(3) Principal piece mask. The head mask (Fig. 1A, iii) was dilated by a total of 13 pixels (Fig. 1A, iv) in order cover the midpiece area and then it was subtracted from the entire sperm mask (Fig. 1A, i), resulting in a mask corresponding to principal piece only (Fig. 1A, v).
(4) Midpiece mask. To create this mask, we subtracted the principal piece mask (Fig. 1A, v) from the entire sperm mask (Fig. 1A, i), resulting in a mask including head and midpiece (Fig. 1A, vi). Subsequently, we subtracted the one pixel dilated version of head mask (Fig. 1A, iii) to obtain a mask for the midpiece region (Fig. 1A, vii). Finally, we eroded one pixel from the latter mask to remove incomplete pixels (Fig. 1A, viii), and we dilated it by two pixels to include all the pixels that correspond to the midpiece (Fig. 1A, ix).
(5) Tail mask. To evaluate the changes in the whole tail region, we created a new mask combining the mid and principal piece masks.

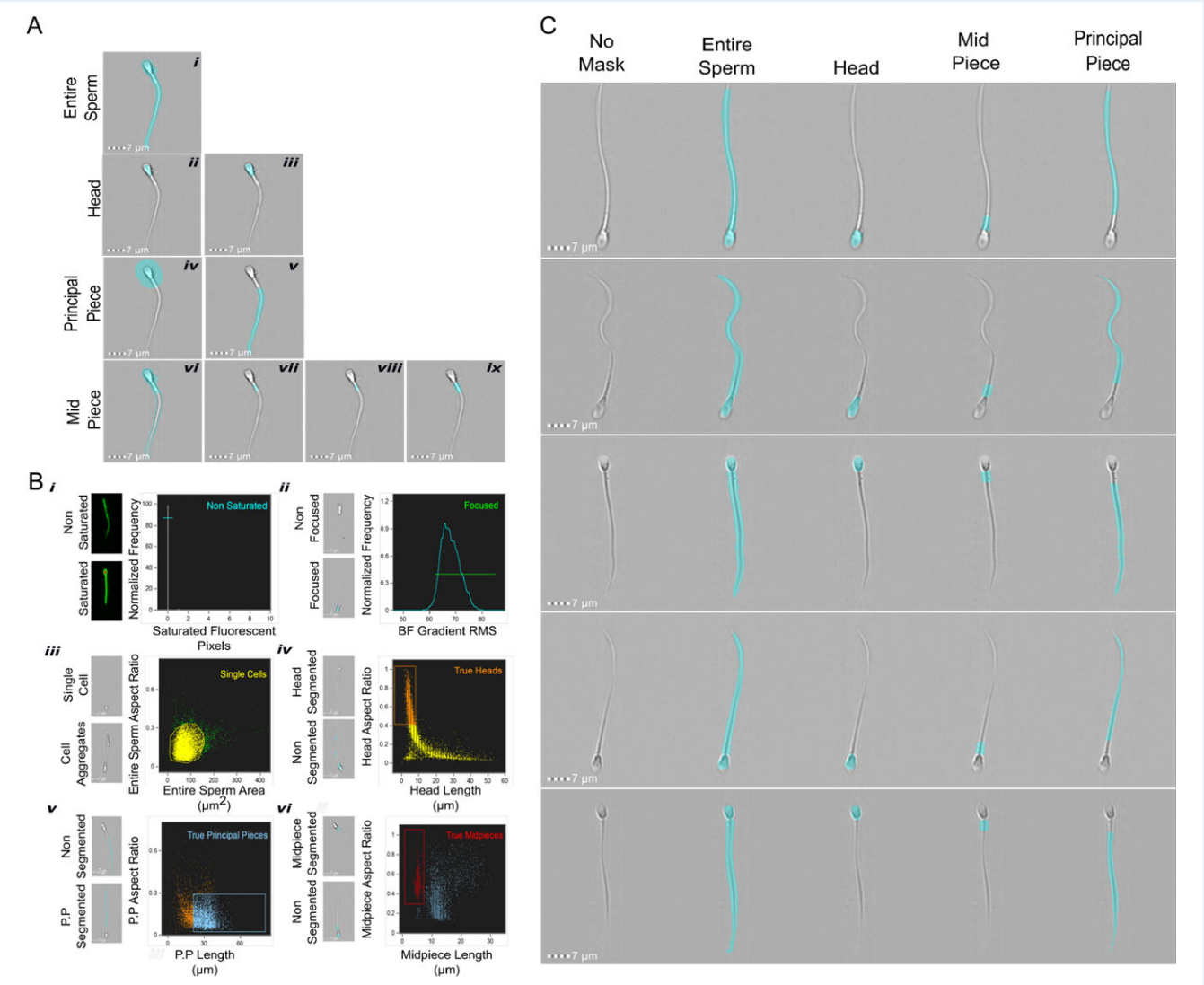

Figure 1 Sperm segmentation and population selection procedures. (**A**) Steps used to obtain the different masks for sperm segmentation: entire sperm, one pixel erosion of morphology function mask in bright-field images (i); head mask: detection of round regions function were through adaptive erode function (ii), and two pixels dilatation to detect the head properly (iii). Principal piece segmentation: ten pixels dilatation of mask in iii (iv), subtraction of the mask in iv from the mask in i to obtain the final Principal Piece mask (v). Midpiece: the mask in v was subtracted from the mask in i (vi), then the mask in v were subtracted from the last mask (vii). The resulting mask was eroded one pixel (viii), and finally a two pixel dilatation was applied to viii in order to obtain the final midpiece mask (ix). (**B**) Different plots used to select the final population for further fluorescence analysis. Histogram to detect saturated pixels to exclude saturated images (i). Histogram of gradient RMS in Ch01 to eliminate out of focus cells (ii). Bivariate plot of Area versus Aspect Ratio parameters to discriminate cell aggregates (iii). Bivariate plots to select images properly segmented (iv–vi). Representative images are shown to the left of each plot. (**C**) Representative images of the populations to demonstrate the accuracy of the segmentation and gating process.

Populations selection

The first step was to exclude the images with saturated pixels (if any). The images were acquired with a pixel depth of 12 bit, in other words, pixel display gray-intensity values between 0 and 4095, where higher pixel values indicate saturated pixels for exclusion of images from the analysis. The number of saturated pixels was calculated for each image using the entire sperm mask, and this quantification was plotted in a histogram; only those images that do not present pixels with values higher than 4085 (i.e. saturated pixels) were selected (Fig. 1B, i, cyan population), and those images with one or more saturated pixels were excluded. Since we excluded saturated images during acquisition, a common histogram cannot be observed in Fig. 1B, i; instead a single line indicates that almost 100% of the images were not saturated. Once we obtained only non-saturated images, we continued with the exclusion of out-of-focus images using the Gradient Root Mean Square (RMS) feature which is a common way to define the focus of an image. This feature measures the quality of an image by detecting large changes in pixel values. The value of gradient RMS is obtained using the average gradient of a pixel normalized for variations in intensity level (Peli, 1990). A focused image will display a high value of gradient RMS due the high difference in gray-intensity values between the image (i.e. the sperm) and the background. The threshold value for selected focused images were obtained empirically and it was set to 62. In this case, images

with values higher than 62 were considered to be in focus (Fig. 1B ii, green population). Most of the images in the analysis were both, non-saturated and focused because we selected these images during acquisition. When the focused and non-saturated images where selected, we proceeded to gate those images which contained only single cells, excluding cellular aggregates, debris or non-sperm images. For this purpose, those cells with an area between 50 and 200 μm^2, and an aspect ratio value lower than 0.3 were selected (Fig. 1B, iii, yellow population).

Next, it was necessary to select the images which were properly segmented. Starting with the selected population, and using specific features created for each mask, we selected the images with accurate head segmentation. Those cells with a head aspect ratio lower than 0.4 and a head length higher than 10 µm were excluded (Fig. 1B, iv, orange population). To select those images with correct principal piece segmentation, we plotted the aspect ratio versus the length of the principal piece mask of the images in the True Heads population (Fig. 1B, iv, orange population). The cells with an aspect ratio lower than 0.3 and a length higher than 20 µm were gated as True Principal Pieces (Fig. 1B, v, light blue population). Finally, the cells with proper head and principal piece segmentation were used to select the cells with an accurate midpiece identification. Those sperm with a midpiece smaller than 8 µm and an aspect ratio higher than 0.35 were gated as True Midpieces (Fig. 1B, vi, red population). After using all these filters, the resulting images were used to proceed with the fluorescence quantification of each segment and statistical analysis. Figure 1C shows representative images of this population to demonstrate the accuracy of the segmentation and gating process. After applying all segmentation and depuration steps, we obtained around 2000 images properly processed per condition for further analysis (data not shown). To obtain this number of analyzable images, we normally acquired 10 000 events per condition.

SDS-PAGE and immunoblotting

We followed the procedure previously described by Alvau *et al.* (2016). Briefly, sperm were collected by centrifugation, washed in 1 ml of PBS, resuspended in Laemmli sample buffer (Laemmli, 1970) without addition of β-mercaptoethanol, boiled for 5 min and centrifuged at 12 100 *g*. Supernatants were then supplemented with 5% (*v*/*v*) β-mercaptoethanol and boiled once more for 3 min. Protein extracts were analyzed by SDS-PAGE and then electro-transferred to PVDF (Bio-Rad). PVDF membranes were blocked with 5% fat-free milk in TBS containing 0.1% Tween 20 (T-TBS) and the anti-Fer (5E2) antibody that was used at a final concentration of 1:1000. The secondary antibody was diluted in T-TBS (1:10 000). Enhanced chemiluminescence ECL Plus Kit (GE Healthcare, USA) was used for protein detection.

Immunofluorescence

After swim-up in NC conditions, sperm were centrifuged at 800 *g* for 5 min, washed with 1 ml PBS, and centrifuged again at 800 *g* for 5 min. Sperm were fixed in solution by adding 4% (*v*/*v*) paraformaldehyde in PBS for 10 min at room temperature. Then sperm were centrifuged at 800 × g for 5 min, washed with 1 ml PBS, centrifuged at 800 *g* for 5 min and resuspended in 500 µl PBS. A 50 µl drop of this suspension was placed in polylysine-coated coverslips (Corning #1.5) and let to dry in air. Non-bound cells were removed by washing with PBS. Cells were then permeabilized with 0.5% (*v*/*v*) Triton X-100 in PBS for 5 min at room temperature and washed three times for 5 min with T-PBS (0.1% (*v*/*v*) Tween 20 in PBS). Samples were blocked with 3% (*w*/*v*) BSA in T-PBS for 1 h at room temperature and then incubated with anti-FER antibody (clone 5D2) 1:50 diluted in 1% (*w*/*v*) BSA overnight at 4°C in a humidifier chamber. After incubation, sperm were washed three times for 5 min with T-PBS and incubated with Alexa 488-conjugated secondary antibody (1:200) diluted in T-PBS containing 1% (*w*/*v*) BSA for 1 h at room temperature. Finally, samples were washed three times for 10 min with T-PBS and the coverslips were mounted using Vectashield H1000 (Molecular Probes, USA). Epifluorescence microscopy was used (TE300 Eclipse microscope, Nikon, Japan) with an oil immersion objective (Nikon, ×60, NA1.4) coupled with a CMOS camera (Zyla 4.2, Andor, UK). Negative controls using a secondary antibody alone were performed to check for specificity.

Statistical analysis

Data analyses were performed by means of the RStudio software, v1.0143 (R Core Team, 2016). All data were verified to accomplish the parametric assumptions of homogeneity of variances and normality. The box plot graphics were performed with the package ggplot2 (Wickham, 2009); the whiskers in the boxes represent the dispersion of data according to Tukey's definition i.e. the whiskers extend to data points that are <1.5 × interquartile range away from first/third quartile. Data above or below these values were considered as outliers. When notches in boxes do not overlap, the medians could be judged to differ significantly ($P < 0.05$), whereas overlapping did not rule out a significant difference (Krzywinski and Altman, 2014).

Results

Segmentation process enable unbiased measurement of the flagellum predominant increase in pY during capacitation

Motile sperm cells were recovered by 1-h swim-up in NC media or capacitated media. Immediately after recovery, cells were fixed to proceed for pY staining, and labeled as NC or 1 h (capacitation), respectively. Another sample was incubated further under capacitating conditions for 17 h (corresponding to 18 h of capacitation). The three types of samples were processed for pY staining according to the technique described above. The sperm pY labeling was detected using an Image-based flow cytometer as described in the materials and methods section and Figure 1. As previously reported, pY increases during capacitation. The advantage of this methodology is that it detects the pY changes in different subcellular areas (Fig. 2). Non-capacitated sperm presented no staining at all or staining only in the head, either over the acrosome or the equatorial segment (Fig. 2A, i–iii) and rarely in the acrosome and midpiece (Fig. 2A, iv), but not in the principal piece. After 1 h in capacitating conditions, pY was clearly observed in the principal piece, combined (Fig. 2A, vi–viii) or not with head staining (Fig. 2A, v). This pY staining was more intense after 18 h of capacitation in the principal piece (Fig 2A, ix; C; F), combined (Fig. 2A, x and xii) or not with head staining (Fig 2A, ix and xi). Using the head and tail masks (see above), we constructed dot plots to quantify the fluorescence intensity of the different subcellular sperm regions and the percentage of cells in each condition showing no staining (no pY), staining only in the head, tail or both in the head and tail. Most cells incubated in NC conditions (57.9%) did not present pY (Fig. 2B, i) or displayed only head labeling (20.4%). After 1 h of capacitation, the sperm population with no pY label significantly decreased (33.7%), and the percentage of cells with head and tail labeling increased ~5-folds (from 3.8 to 24.5%) (Fig 2B, ii). After 18 h in capacitation-supporting conditions, the majority of cells were those with pY only in the tail followed by those with pY in head and tail (47.4 and 40.1%, respectively) (Fig 2B, iii). Not only did the number of pY positive cells increase during capacitation but also the

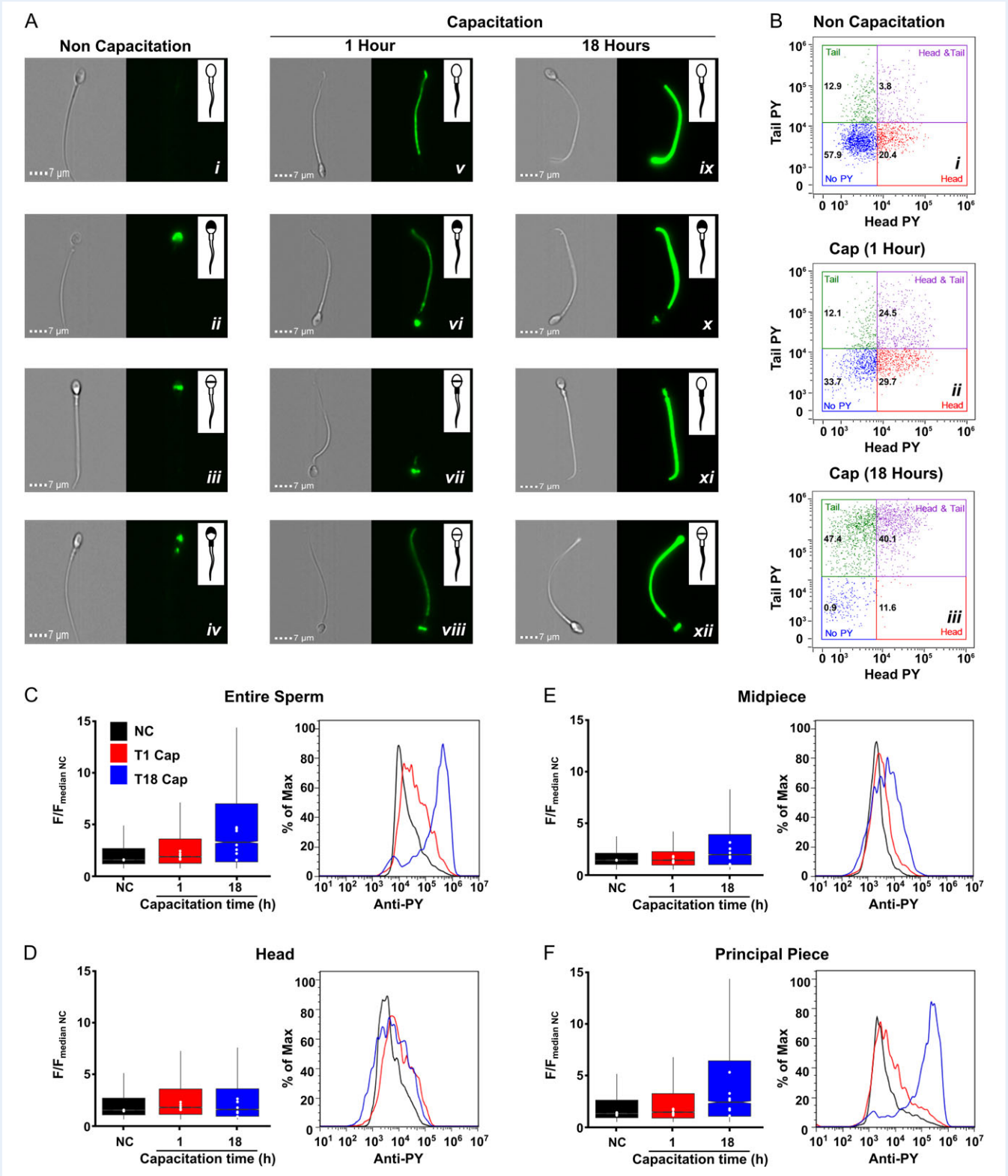

Figure 2 Segmentation process enable unbiased measurement of the flagellum predominant increase in pY during capacitation. (**A**) Representative brightfield and fluorescence (pY staining) images of sperm non-capacitated (NC) (left), or capacitated for 1 h (middle) or 18 h (right), showing the different staining patterns observed in each condition. The inset illustrates the region of the cell where pY staining is observed and exemplifies the different staining patterns. Clearly, capacitation-induced pY particularly in the principal piece of the flagella. (**B**) Two-dimensional fluorescence plots comparing the subcellular fluorescence intensity from representative samples of non-capacitated sperm (i), or sperm capacitated for 1 h (ii) or 18 h (iii). The numbers in each quadrant represent the percentage of cells for each staining pattern. (**C–F**). Box plots of normalized pY fluorescence

intensity of labeling appeared to be increased in the capacitated sperm population.

Capacitation induces pY primarily in the principal piece

Although it has been previously reported that capacitation increases pY mainly in the principal piece of the flagella (Carrera *et al.*, 1996; Alvau *et al.*, 2016), the number of cells that can be analyzed using immunocytochemistry is rather small (<200). Attempts at pY quantification have been performed using the *H*-score, which is basically a classification of the fluorescence intensity performed by the experimenter (Sagare-Patil and Modi, 2017). Our experimental design and mask based analysis allowed us to identify and quantify pY staining in the different sperm regions using an unbiased approach by quantifying pixel values. We applied the masks to all images and obtained fluorescence intensity values for each region of every cell (~2000 cells per experiment). Since fluorescence intensity varies among experiments, the comparison between treatments was performed by normalizing each group to the NC condition. For this purpose, the fluorescence intensity value for each region of every cell was divided by the mean fluorescence (of all cells in that experiment) of the corresponding region for the NC condition. Figure 2 shows box plots of these values (*F*/FmeanNC) for the entire sperm (2 C), the head (2D), the midpiece (2E) and the principal piece (2 F) for NC (initial condition) and 1 and 18 of capacitation. When the entire sperm was analyzed, a slight but significant pY increase was observed after 1 h of capacitation, which was dramatically enhanced after 18 h of capacitation. On the other hand, when the analysis was performed in separate compartments, a clear increase of pY in the principal piece was observed, especially after 18 h. Histograms of each condition of a representative experiment are shown to the right of every panel (Fig. 2B–E). Since pY in the head and midpiece was practically constant during capacitation, we decided to focus our attention in the principal piece for the next set of experiments.

Segmentation strategy can be used to analyze signaling in human spermatozoa: the capacitation-associated increase in human sperm pY is reduced by PF431396 but not by PF573228

By using Western blot analyses, it has been shown that PF431396 blocks the increase of pY in horse (González-Fernández *et al.*, 2013), human (Battistone *et al.*, 2014) and mouse (Alvau *et al.*, 2016) spermatozoa. However, the method used in those studies was silent regarding how the inhibitor affected pY in different sperm compartments. To analyze compartmentalization of the PF431396 inhibition, the newly developed segmentation strategy using image-based flow cytometry was employed (Fig. 3). PF431396 is usually used as a FAK-family tyrosine kinase inhibitor however it blocks both members of the FAK-family (FAK and PYK2) with similar IC50 and recent experiments from our laboratory showed that this inhibitor can also block FER tyrosine kinase with a similar IC50 (Alvau *et al.*, 2016). To differentiate between the tyrosine kinases, PF573228 was also evaluated. The latter inhibitor was one order of magnitude more efficient against FAK when compared with PYK2 (Alvau *et al.*, 2016). Interestingly, PF431396 reduced the increase in pY only in the sperm flagellum and not in the head. These experiments suggest that different tyrosine kinases are responsible for the pY in the head and in the flagella of human sperm. On the other hand, the lack of effect of PF573228 implies that FAK is not involved in the regulation of the pY increase in human sperm. Moreover, we also showed that while sperm from PYK2 knock-out mice display normal levels of pY during capacitation, sperm from mice in which FER was replaced by a non-functional kinase mutant are unable to undergo pY. These experiments indicated that FER is the enzyme responsible for the capacitation-associated increase in pY in mice.

Expression of FER in human spermatozoa

To evaluate the presence and localization of FER kinase in human sperm, Western blot analysis (Fig. 4A) and immunofluorescence (Fig. 4B) were conducted. These experiments revealed that the short splicing variant (~50 KDa) of FER kinase, denominated FERT, was present in human sperm extracts and it was localized along the flagellum of human sperm.

The specificity of this antibody has been previously validated using the FERDR/DR genetic mouse model. The DR mutation in FER renders the kinase inactive and unstable; therefore, the mice model lacks FER and FERT protein (Alvau *et al.*, 2016).

Discussion

Protein phosphorylation in tyrosine residues has been a hallmark to define sperm capacitation. This protein modification has been proposed to play a role in sperm motility of several species. The methodology developed in this work provides several advantages to traditional techniques used for this purpose. In general, pY is measured using Western Blot analysis, a technique that allows quantification of the levels of phosphorylation providing an average result of a heterogeneous population. However, it does not provide information about the subcellular region where pY is taking place. Immunocytochemistry has been used to locate the subcellular sites of pY with the disadvantage that a very small number of cells can be analyzed and an accurate fluorescence quantification is not possible. Godbole *et al.* (2007) proposed the use of the *H*-score to quantify the levels of pY in human sperm, however, this method relies on the classification of the fluorescence intensity (no staining, weak, medium or maximum) by means of a subjective observation of the experimenter determined in a small number of cells (>200). In this work, we applied image-based flow cytometry to establish a method to analyze sperm, either the whole cell or three segmented regions. After the segmentation procedure, the intensity of fluorescence labeling can be detected and quantified in

(F/FmedianNC) summarize the fluorescence intensity under the three experimental conditions, NC (initial condition), 1 and 18 h of capacitation, for the entire sperm (**C**), the head (**D**), the midpiece (**E**) and the principal piece (**F**). Data include measurements of seven independent experiments performed with ejaculates from different donors. Each white dot represents the median value of each donor in each condition (n = ~2000 cells per donor), each box contains at least 14 000 cells. A representative histogram of one experiment is shown to the right. Notches do not overlap ($P < 0.05$).

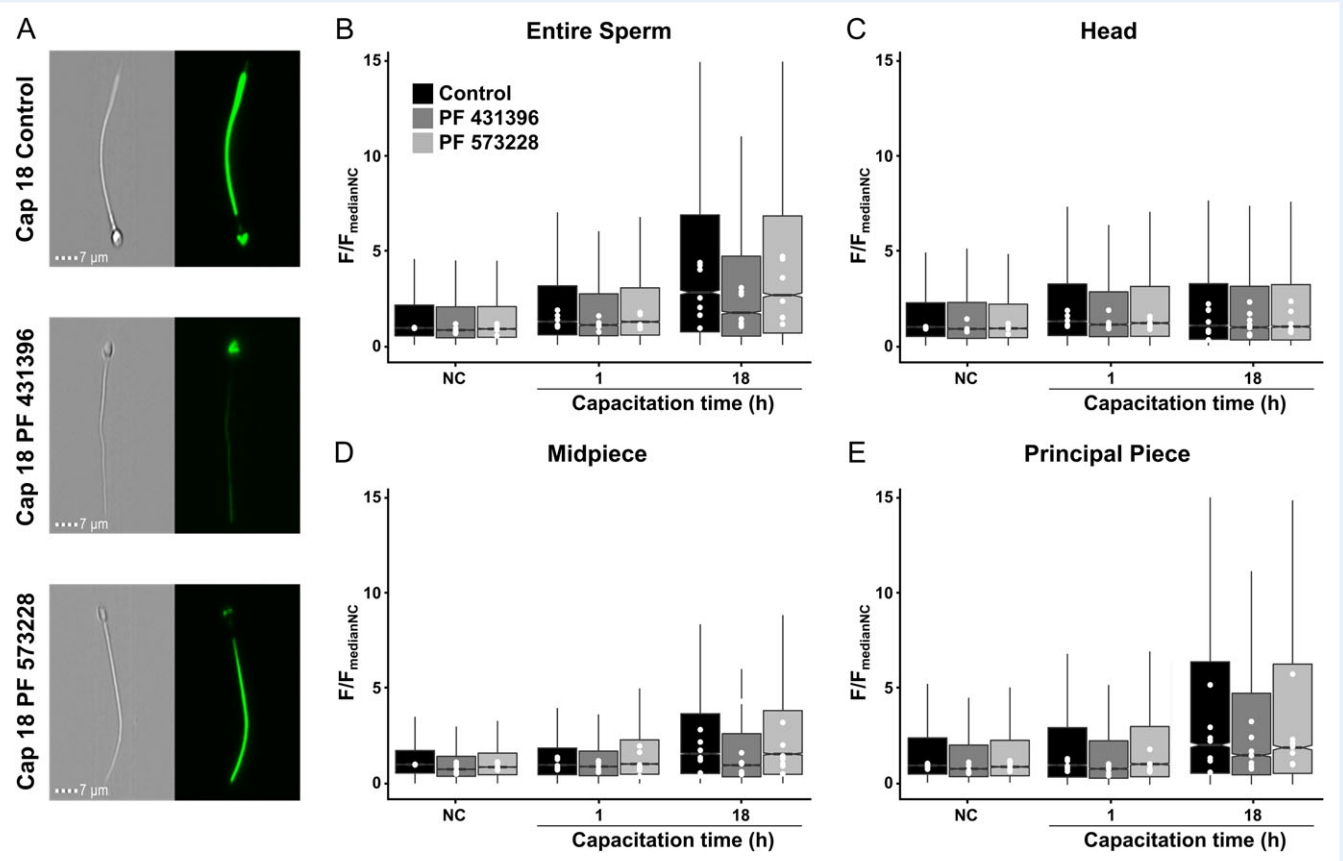

Figure 3 Inhibition of PY is reduced by an inhibitor of FER, FAK and PYK2 but not by an inhibitor of FAK. Sperm cells were incubated under non-capacitating conditions (NC) or capacitated for 1 or 18 h. Representative brightfield and fluorescence (pY staining) images of sperm capacitated for 18 h showing the different staining observed in the absence of presence of inhibitors for FER/FAK/PYK2 (PF431396) or FAK (PF573228) (**A**). After incubation, the levels of pY were evaluated for the entire sperm (**B**), the head (**C**), midpiece (**D**) and principal piece (**E**). Box plots of normalized pY fluorescence (F/FmedianNC) summarize the fluorescence intensity under different incubation conditions and in the absence of presence of inhibitors. PF431396 produced a slight decrease of the fluorescence intensity of non-capacitated cells in comparison to control conditions for entire sperm, midpiece and principal piece, leaving the head with identical levels. This decrease was observable after the first hour of capacitation, in this case for all the sperm regions. At 18 h of capacitation, the effect of this inhibitor was more prominent for the entire sperm the midpiece and the principal piece. The levels of pY in the head were not altered by this inhibitor. In contrast, PF573228 did not produce a significant effect in the pY levels in any condition or segment of the cell. Data include measurements of seven independent experiments performed with ejaculates from different donors. Each white dot represents the median value of each donor in each condition (n = ~2000 cells per donor). Each box represents at least 14 000 cells. Notches do not overlap ($P < 0.05$).

the different regions. In this work we utilized this process to analyze pY in a large number of cells, confirming that sperm cells are differentially labeled during capacitation. Our method provides an alternative strategy to study pY in a fast and quantitative manner that can be applied, for instance, to elucidate the signaling cascade leading to capacitation induced by pY in human sperm. This is particularly important since genomic manipulation strategies cannot be applied in humans. As our segmentation strategy depends only on non-stained bright-field images, it can be applied to study the expression of other proteins of interest, or even be used to study intracellular parameters in living cells that can be followed using fluorescent dyes sensitive to other parameters. Additionally, the image-based flow cytometry offers the opportunity of multiparametric analysis due to the multiples fluorescence detectors present in the system, it means we can analyze up to nine parameters using an adequate combination of fluorescent dyes for live or fixed cells. Moreover, as this procedure depicted here could be stored as a template file, it can be applied to each experiment to produce the segmentation of sperm images without changes to the threshold parameters, which saves considerable time.

Although proteomic studies have revealed the presence of a large list of kinases and phosphatases in sperm from different species (Urner and Sakkas, 2003), the exact kinases involved in the capacitation-induced increase in pY has been difficult to establish. As a result of pharmacological and immunological studies, several candidates have been proposed to play a role in this process, including SRC (Baker *et al.*, 2006; Varano *et al.*, 2008; Krapf *et al.*, 2010), FYN (Luo *et al.*, 2012), ABL (Baker *et al.*, 2009), FAK and PYK2 (González-Fernández *et al.*, 2013; Battistone *et al.*, 2014). Recently, our group (Alvau *et al.*, 2016) reported that PF431396 (a FAK and PYK2 inhibitor) but not PF573228 (a more specific inhibitor for FAK), inhibited pY during mouse sperm capacitation. Although these results suggested a role for

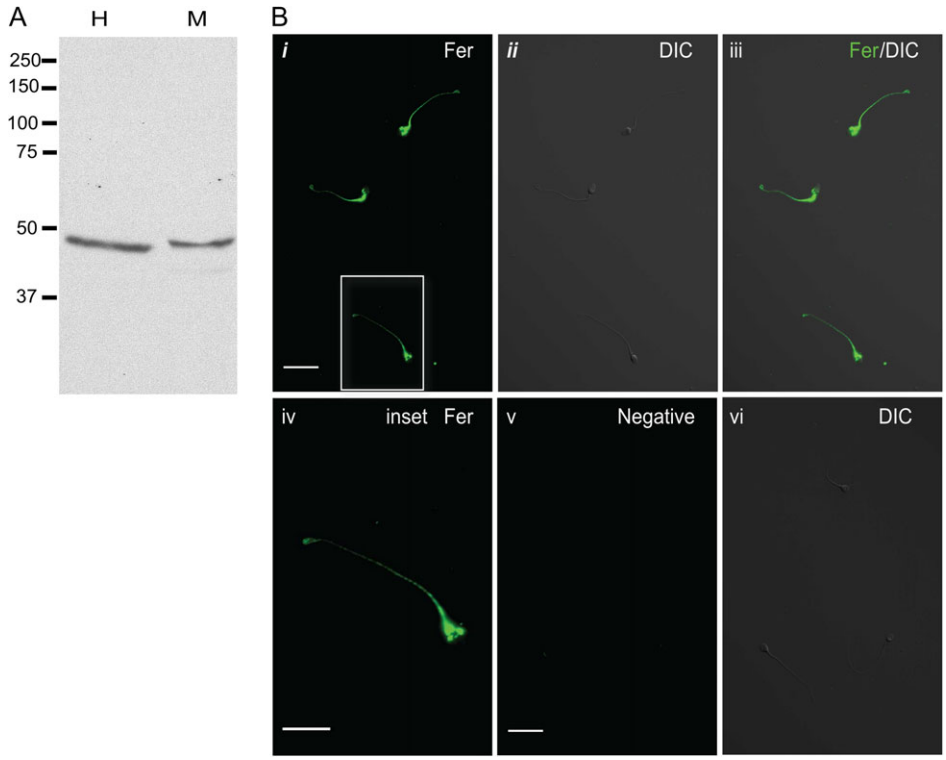

Figure 4 FER localizes mainly in the flagellum of human sperm. (**A**) Protein extracts from human (H) sperm were analyzed by western blotting using anti-FER antibody. Mouse (M) sperm protein extracts were included as a control. Only the short isoform of FER (FERT) was detected in both species. (**B**) Immunolocalization of FER in human sperm. Human sperm were fixed, permeabilized, treated with 3% BSA and probed with anti-FER antibody (1:50). Alexa 488-conjugated secondary antibody (1:200) was used. (i) Fluorescence image illustrating staining with FER antibody in human sperm, scale bar: 20 μm; (ii) DIC image corresponding to the image in panel i; (iii) merged image of FER fluorescent staining and DIC; (iv) fluorescent image of the corresponding inset in panel i, scale bar: 5 μm; (v) negative control: fluorescence image after incubation with secondary antibody alone, scale bar: 20 μm; (vi) DIC image corresponding to the image in panel (v). Western blots and images shown are representative of three independent experiments with similar results.

PYK2 in sperm tyrosine phosphorylation, sperm from Pyk2−/− mice showed completely normal pY during capacitation. As many other small molecule inhibitors, which are known to have off-target effects, PF431396 was shown to block FER *in vitro* with a similar IC50 to that found for FAK-family tyrosine kinases. In addition, a small molecular weight splicing variant of FER known as FERT is present in mouse sperm (Alvau *et al.*, 2016). Moreover, in sperm from mice in which the FER gene was replaced with a kinase-dead mutant of FER, the pY was not increased. Altogether, these results demonstrated that FERT is the tyrosine kinase responsible for the increase in tyrosine phosphorylation during capacitation in mouse sperm. In addition, we showed that FERT is also present in human sperm with a probable role on human sperm capacitation-induced tyrosine phosphorylation. Since in human sperm, it is not possible to conduct genetic loss-of-function experiments, we cannot definitely discard a role for other tyrosine kinases also known to be present in these cells, such as PYK2.

In conclusion, segmentation of sperm images obtained by image-based flow cytometry is a versatile method that can be exploited to study several features of sperm physiology and for the establishment of high-throughput assays.

Acknowledgments

The authors thank Andres Saralegui, Jose Luis De la Vega, Shirley Ainsworth, Juan Manuel Hurtado, Roberto Rodríguez, David Castañeda, Omar Arriaga and Arturo Ocádiz for technical assistance. L.C.G is researcher from the Consejo Nacional de Investigaciones Científicas y Técnicas (Argentina). A.M.I. is a PhD student of the Universidad Nacional de Córdoba (Argentina) and fellowship holders from Consejo Nacional de Investigaciones Científicas y Técnicas (Argentina).

Authors' roles

A.M.V., A.M.I. and C.L.T. conceived the question and design the experiments. A.M.V., A.M.I., M.G.G. and P.T.R. performed the experiments and analyzed the data. P.T.R. and A.M.I. prepared the final version of the figures. A.M.V. and A.M.I. applied statistical analysis and validation. C.L.T., A.M.V., P.E.V. and L.G. wrote the article, C.L.T., P.E.V. and L.G. obtained funding. All authors contributed to the construction of the article and agreed with the final version.

Funding

Dirección General de Asuntos del Personal Académico (DGAPA-IN203116 to C.T.) Fronteras-Consejo Nacional de Ciencia y Tecnología (CONACyT) No. 71 to C.T. and Eunice Kennedy Shriver National Institute of Child Health and Human Development NIH (RO1 HD38082) to P.E.V. and by a Lalor Foundation fellowship to M.G.G. A.M. is a student of the Maestría en Ciencias Bioquímicas-Universidad Nacional Autónoma de México (UNAM) program supported by CONACyT (416400) and DGAPA-UNAM. A.M. obtained a scholarship from Red MacroUniversidades.

Conflicts of interest

The authors declare that they have no conflicts of interest.

References

Alvau A, Battistone MA, Gervasi MG, Navarrete FA, Xu X, Sánchez-Cárdenas C, De la Vega-Beltran JL, Da Ros VG, Greer PA, Darszon A *et al*. The tyrosine kinase FER is responsible for the capacitation-associated increase in tyrosine phosphorylation in murine sperm. *Development* 2016;**143**:2325–2333.

Austin CR. Observations of the penetration of sperm into the mammalian egg. *Aus J Sci Res* 1951;**4**:581–596.

Baker MA, Hetherington L, Aitken RJ. Identification of SRC as a key PKA-stimulated tyrosine kinase involved in the capacitation-associated hyperactivation of murine spermatozoa. *J Cell Sci* 2006; **119**:3182–3192.

Baker MA, Hetherington L, Curry B, Aitken RJ. Phosphorylation and consequent stimulation of the tyrosine kinase c-Abl by PKA in mouse spermatozoa; its implications during capacitation. *Dev Biol* 2009;**333**:57–66.

Battistone MA, Alvau A, Salicioni AM, Visconti PE, Da Ros VG, Cuasnicú PS. Evidence for the involvement of proline-rich tyrosine kinase 2 in tyrosine phosphorylation downstream of protein kinase A activation during human sperm capacitation. *Mol Hum Reprod* 2014;**20**:1054–1066.

Chang MC. Fertilizing capacity of spermatozoa deposited into the fallopian tubes. *Nature* 1951;**168**:697–698.

Carrera A, Moos J, Ning XP, Gerton GL, Tesarik J, Kopf GS, Moss SB. Regulation of protein tyrosine phosphorylation in human sperm by a calcium/calmodulin-dependent mechanism: identification of a kinase anchor proteins as major substrates for tyrosine phosphorylation. *Dev Biol* 1996;**180**:284–296.

Godbole GB, Modi DN, Puri CP. Regulation of homeobox A10 expression in the primate endometrium by progesterone and embryonic stimuli. *Reproduction* 2007;**134**:513–523.

González-Fernández L, Macías-García B, Loux SC, Varner DD, Hinrichs K. Focal adhesion kinases and calcium/calmodulin-dependent protein kinases regulate protein tyrosine phosphorylation in stallion sperm. *Biol Reprod* 2013;**88**:138: 1–12.

Kennedy CE, Krieger KB, Sutovsky M, Xu W, Vargovič P, Didion BA, Ellersieck MR, Hennessy ME, Verstegen J, Oko R *et al*. Protein expression pattern of PAWP in bull spermatozoa is associated with sperm quality and fertility following artificial insemination. *Mol Reprod Dev* 2014; **81**:436–449.

Krapf D, Arcelay E, Wertheimer EV, Sanjay A, Pilder SH, Salicioni AM, Visconti PE. Inhibition of Ser/Thr phosphatases induces capacitation-associated signaling in the presence of Src kinase inhibitors. *J Biol Chem* 2010;**285**:7977–7985.

Krzywinski M, Altman N. Visualizing samples with box plots. *Nat Methods* 2014;**11**:119–120.

Laemmli UK. Cleavage of structural proteins during the assembly of the head of bacteriophage T4. *Nature* 1970;**227**:680–685.

Luo J, Gupta V, Kern B, Tash JS, Sanchez G, Blanco G, Kinsey WH. Role of FYN kinase in spermatogenesis: defects characteristic of Fyn-Null sperm in mice1. *Biol Reprod* 2012;**86**:1–8.

Mata-Martínez E, José O, Torres-Rodríguez P, Solís-López A, Sánchez-Tusie AA, Sánchez-Guevara Y, Treviño MB, Treviño CL. Measuring intracellular Ca2+ changes in human sperm using four techniques: conventional fluorometry, stopped flow fluorometry, flow cytometry and single cell imaging. *J Vis Exp* 2013;**75**:e50344.

Peli E. Contrast in complex images. *J Opt Soc Am A* 1990;**10**:2032–2040.

R Core Team *R: A Language and Environment for Statistical Computing*. Vienna, Austria: R Foundation for Statistical Computing, 2016. https://www.R-project.org/.

Sagare-Patil V, Modi D. Identification of motility-associated progesterone-responsive differentially phosphorylated proteins. *Reprod Fertil Dev* 2017; **29**:1115–1129.

Santiani A, Ugarelli A, Evangelista-Vargas S. Characterization of functional variables in epididymal alpaca (Vicugna pacos) sperm using imaging flow cytometry. *Anim Reprod Sci* 2016;**173**:49–55.

Urner F, Sakkas D. Protein phosphorylation in mammalian spermatozoa. *Reproduction* 2003;**125**:17–26.

Varano G, Lombardi A, Cantini G, Forti G, Baldi E, Luconi M. Src activation triggers capacitation and acrosome reaction but not motility in human spermatozoa. *Hum Reprod* 2008;**23**:2652–2662.

Visconti PE, Krapf D, la Vega-Beltran JL, de Acevedo JJ, Darszon A. Ion channels, phosphorylation and mammalian sperm capacitation. *Asian J Androl* 2011;**13**:395–405.

Wickham H *ggplot2: Elegant Graphics for Data Analysis*. New York: Springer-Verlag, 2009. https://ggplot2.org.

World Health Organization *WHO Laboratory Manual for the Examination and Processing of Human Semen*, 5th edn. Geneva, Switzerland: WHO Press, 2010.